MULTIAXIAL FATIGUE TESTING AND ANALYSIS OF METALLIC MATERIALS

L. Reis, Bin Li and M. de Freitas

Department of Mechanical Engineering
Instituto Superior Técnico, Av. Rovisco Pais, 1049-001, Portugal

Resumo. De modo a analisar o comportamento dos materiais em fadiga multiaxial realizou-se uma série de testes utilizando uma máquina servo-hidraulica biaxial (8800 Instron). O material utilizado foi o aço 42CrMo4, temperado e revenido (500ºC). Foram consideradas seis trajectorias de carregamento, compostas por tracção/torção ciclicas. O objectivo é obter vidas experimentais em fadiga multiaxial para o mesmo estado final tensão extensão realizado por diferentes trajectorias de carga. As respostas locais cíclicas elasto-plásticas de tensão-deformação são analisadas utilizando o programa comercial de elementos finitos ABAQUS. È apresentado o método computacional utilizado para estimar/avaliar as vidas obtidas experimentalmente. Com base nas respostas locais cíclicas elasto-plásticas de tensão-deformação, os parâmetros de dano em fadiga multiaxial com base na deformação são aplicados para correlacionar com as vidas obtidas experimentalmente. Para comparação utiliza-se a abordagem da Menor Elipse Circunscrita (MEC). A comparação mostra que o procedimento, tendo em conta os factores de não proporcionalidade, e a gama de deformação equivalente correlacionam bem com os resultados experimentais obtidos neste estudo.

Abstract. In order to analyse the multiaxial fatigue behaviour of metallic materials, a series of tests were carried out using a biaxial servo-hydraulic machine (8800 Instron). A low alloy steel 42CrMo4 heat treated, quenched and tempered (500ºC) was used in this study. Six loading paths composed of tension/compression and torsion for different waveforms and phase shifts between tension and torsion were tested. The objective is to obtain experimental fatigue lives for the same final stress strain state reached by different loading paths. The local cyclic elastic-plastic stress-strain responses are analysed using commercial ABAQUS finite element program. Based on the local cyclic elastic-plastic stress-strain responses, the strain-based multiaxial fatigue damage parameters are applied to correlating the experimentally obtained lives. As a comparison, a stress-invariants based approach with the Minimum Circumscribed Ellipse (MCE) approach for evaluating the effective shear stress amplitude is also applied for fatigue life prediction. The comparison shows that both the equivalent strain range and the stress-invariant parameter with non-proportional factors can correlate well the experimental results obtained in this study.

1. INTRODUCTION

Machine components and structures in service are generally subjected to multiaxial fatigue loading conditions. For example, rotor shafts in electric power plants, propeller shafts in ships, and so on. Fatigue life evaluation of mechanical components under complex loading conditions is of great importance to optimise structural design, and improve inspection and maintenance procedures.

Fatigue life generally consists of three stages: crack initiation, crack propagation and final fracture. For engineering design, crack initiation life is commonly defined as crack nucleation and small crack growth to NDT detectable crack size. Different mechanisms and controlling parameters dominate the fatigue life stages. Fatigue design against crack initiation may lead to different material selection criteria and structural design from fatigue design against crack propagation. Therefore, more recent research efforts have been paid for studying the crack initiation behaviour of mechanical components and structures under multiaxial loading conditions.

The problem of the nucleation and growth of small cracks has been conventionally treated in the context of so-called fatigue crack initiation approaches, which are phenomenological stress-life and strain-life equations. When the applied stresses are low and well below the yield stress σ_y of the material under high-cycle fatigue (HCF) conditions, the stress-based approach is used in general. When the applied stresses are quite large, the local plastic strains may be quite large under low-cycle fatigue (LCF) condition and the strain-based approach is more appropriate.

Many experiments have shown that the non-proportional multiaxial loading reduce fatigue life significantly, traditional parameters such as the von Mises equivalent strain range may underestimate the fatigue damage for non-proportional multiaxial loading. In order to treat the non-proportional loading effect on fatigue damage of metallic materials, a lot of multiaxial fatigue models have been proposed in recent years [1], based on the critical plane concept, the integral concept and so on. Some of the recent models require more material parameters and complicated implementation work. Besides, the critical plane concept considers that only the stress/strain states on

the critical plane contribute to fatigue damage, which is criticised by some researchers, since the slipping on all the directions may contribute to fatigue damage.

The objective of the present research is to obtain experimental fatigue lives for the same final stress strain state reached by different loading paths, to study cyclic stress-strain responses behaviour of metallic materials under cyclic tension/compression combined with cyclic torsion loading. A low alloy steel 42CrMo4 heat treated, quenched and tempered (500ºC) was used in this study.

Selected stress-based and strain-based multiaxial fatigue models are applied for correlating the experimental results. Evaluations of the fatigue life prediction approaches are conducted by comparisons of the predicted life with test life. Because the local cyclic stress/strain behaviour is essential parameter for all the fatigue life prediction models, non-linear Finite Element analyses are applied to study the evolution of the local cyclic stress/strain behaviour under various multiaxial loading paths.

2. MATERIAL DATA, SPECIMEN FORM AND TEST PROCEDURE

The material studied in this work is the hard steel 42CrMo4. The mechanical properties are shown in the table 1.

Table 1. Mechanical properties of 42CrMo4 steel

Tensile strength	R_m (MPa)	1100
Yield strength	$R_{p0.2,monotonic}$ (MPa)	980
Elongation	A (%)	16
Young's modulus	E (GPa)	206
Hardness	HV	362

The geometry of the specimen used is shown in Fig. 1.

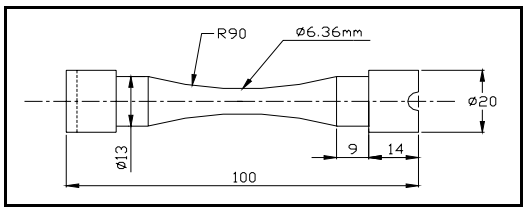
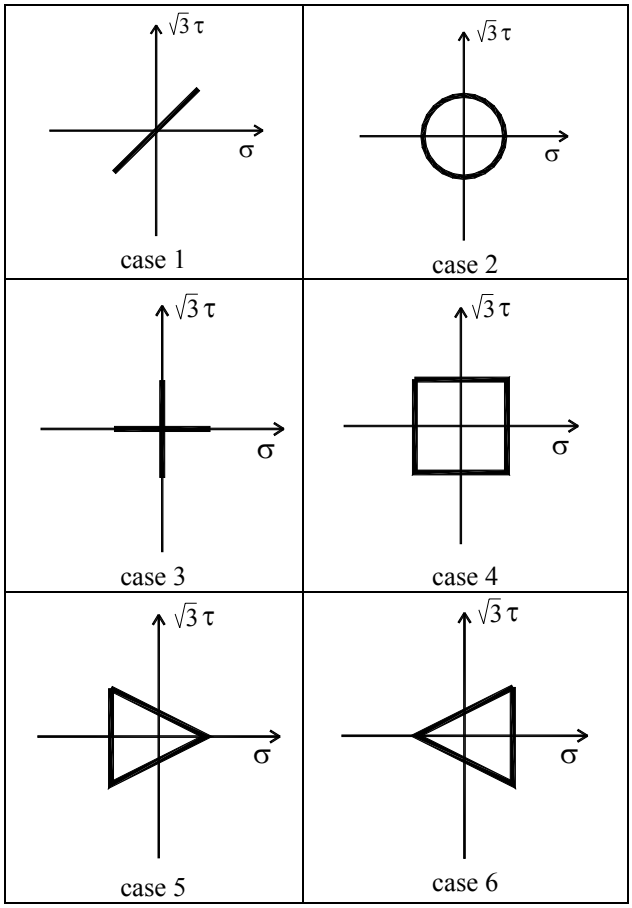


Fig. 1. Geometry and dimensions of the specimen

To study the effects of the loading paths on the additional hardening and fatigue damage, a series of loading paths were applied in the experiments as shown in table 2. The tests performed using a biaxial servo-hydraulic 8800 Instron machine. Test conditions were as follows: frequency 3-5 Hz and room temperature in laboratory air.

Table 2. Multiaxial fatigue loading paths



3. CYCLIC STRESS-STRAIN RESPONSES

When an elastic-plastic material is subjected to cyclic loading, the stress and strain history will initially go through a transient state which asymptotes to a cyclic state. In this cyclic state, the behavior of the body can be characterized by four alternative modes of behaviors [2]: 1- Elastic region. 2-Elastic shakedown. 3-Plastic shakedown. 4- Ratcheting.

Modeling the cyclic behavior of a material subjected to multiaxial elasto-plastic deformation is essential for predicting the fatigue life of components using multiaxial fatigue criteria.

A convenient method of describing the stable material response is through the cyclic stress-strain curve. Generally, a cyclic stress-strain curve is obtained by connecting the tips of stable hysteresis loops for different strain amplitudes of fully reversed strain-controlled tests. This curve originate the so called ´Masing´curve, Eq. (1):

$$\Delta\varepsilon = \frac{\Delta\sigma}{E} + 2\left(\frac{\Delta\sigma}{2K'}\right)^{1/n'} \qquad (1)$$

where K' and n' are the cyclic strength coefficient and cyclic strain hardening exponent, respectively. $\Delta\sigma/2$ and $\Delta\varepsilon/2$ are the stable stress and strain amplitudes, respectively.

Materials whose behaviour differs from the above description are termed ´non-Masing type´. If the response of ´non-Masing´ material deviates significantly, the master curve approach should be used, as described in Ref. [3].

The cyclic properties obtained from fitting the test results are shown in Table 3.

Table 3. Cyclic properties of 42CrMo4 steel ($f=0.2s^{-1}$)

Yield strength	$R_{p,0.2,cyclic}$ (MPa)	540
Strength coefficient	K´(MPa)	1420
Strain hardening exponent	n´	0.12
Fatigue strength coefficient	σ_f'(MPa)	1154
Fatigue strength exponent	b	-0.061
Fatigue ductility coefficient	ε_f'	0.18
Fatigue ductility exponent	c	-0.53

With the uniaxial cyclic stress-strain curve as input, the finite element method is employed to simulate the local elasto-plastic stress-strain responses of the specimen under biaxial loading.

The FE program package ABAQUS is used to solve the cyclic elastic-plastic stress/strain responses. The von Mises yield criterion and the linear kinematic hardening rule are applied for describing the elastic-plastic material properties. Detailed numerical results are presented and discussed in this paper.

4. MULTIAXIAL FATIGUE MODELS FOR CRACK INITIATION LIFE PREDICTION

Many multiaxial fatigue models have been proposed in the last decades, some of the recent models require more material parameters and complicated implementation work. Besides, the critical plane concept considers that only the stress/strain states on the critical plane contribute to fatigue damage, which is criticised by some researchers, since the slipping on all the directions may contribute to fatigue damage.

In this paper, the stress-invariant based and the equivalent strain range based multiaxial fatigue models are selected to correlate the experimental results, because these parameters are average measure of the stress/strain states and should be representative damage parameters. To deal with the non-proportional loading effects, appropriate corrections are applied for these parameters as reviewed in following.

Equivalent Strain Range of ASME Code

The ASME Boiler and Pressure Vessel code Procedure [4] is based on the von Mises hypothesis, but employs the strain difference $\Delta\varepsilon_i$ between time t_1 and t_2:

$$\Delta\varepsilon_{eq} = \frac{1}{(1+v)\sqrt{2}}\left\{\left(\Delta\varepsilon_x - \Delta\varepsilon_y\right)^2 + \left(\Delta\varepsilon_y - \Delta\varepsilon_z\right)^2 + \left(\Delta\varepsilon_z - \Delta\varepsilon_x\right)^2 + 6\left(\Delta\varepsilon_{xy}{}^2 + \Delta\varepsilon_{yz}{}^2 + \Delta\varepsilon_{xz}{}^2\right)\right\}^{1/2} \quad (2)$$

where the equivalent strain range $\Delta\varepsilon_{eq}$ is maximised with respect to time.

Eq. (2) produces a lower equivalent strain range for out-of-phase than the in-phase loading, predicting an increase of the fatigue life, which is in contradiction with experimental results.

An Improved Model Based on the ASME Code

The ASME Code approach expressed in Eq. (2), define a parameter which has a drawback that is, it produces a lower equivalent strain range for non-proportional than the proportional loading, which underestimates the fatigue damage of non-proportional loading, since many recent experiments have shown that the non-proportional loading reduce the fatigue life significantly than the proportional loading with the same loading amplitude.

In this paper, an improved model based on the ASME code approach is proposed by considering the additional hardening and correcting the strain range parameter for non-proportional loading path:

$$\Delta\varepsilon_{NP} = \left(1 + \alpha F_{NP}\right)\Delta\varepsilon_{eq} \quad (3)$$

where F_{NP} is the non-proportionality factor of the loading path, α is a material constant of additional hardening, $\Delta\varepsilon_{eq}$ is the strain range parameter calculated by Eq.(2), and $\Delta\varepsilon_{NP}$ is the corrected strain range parameter.

Eq. (3) is similar with the approach proposed by Itoh et al. [5], but here the MCE (minimum circumscribed Ellipse) approach developed by M. de Freitas et al [6] previously is applied for evaluating the non-proportionality factor of the loading path.

Then the Mason-Coffin formulation can be used for life predictions:

$$\frac{\Delta\varepsilon_{NP}}{2} = \frac{\sigma_f' - \sigma_m}{E}\left(2N_f\right)^b + \varepsilon_f'\left(2N_f\right)^c \quad (4)$$

where σ_m is the mean stress, E is the young's modulus, σ_f' is the fatigue strength coefficient, ε_f' is the fatigue ductility coefficient, and b and c are fatigue strength and fatigue ductility exponents, respectively.

Stress-Invariant Based Approaches

Among many multiaxial models, the Sines [7] and the Crossland [8] are two important criteria, which are formulated by the amplitude of the second deviatoric stress invariant $\sqrt{J_{2,a}}$ and the hydrostatic stress P_H:

$$\sqrt{J_{2,a}} + k(N)P_H = \lambda(N) \tag{5}$$

Crossland suggested using the maximum value of the hydrostatic stress PH,max instead of the mean value of hydrostatic stress PH,m used by Sines in the Eq.(5). A physical interpretation of the criterion expressed as Eq.(5) is that for a given cyclic life N, the permissible amplitude of the root-mean-square of the shear stress over all planes is a linear function of the normal stress averaged over all planes. Besides, from the viewpoint of computational efficiency, the stress-invariant based approach such as Eq.(5) is easy to use and computationally efficient.

In practical engineering design, the Sines and Crossland criteria have found successful applications for proportional multiaxial loading. For non-proportional multiaxial loading, it has been shown that the Sines and Crossland criteria can also yield better prediction results by using improved method MCE for evaluating the effective shear stress amplitude of the non-proportional loading path [6], as described in the following section.

5. MCE APPROACH FOR EVALUATING SHEAR STRESS AMPLITUDE

As discussed in the last section, the evaluation of shear stress amplitude is a key issue for fatigue estimations using Eq. (5). The definition of the square root of the second invariant of the stress deviator is:

$$\sqrt{J_2} \equiv \sqrt{\frac{1}{6}\left\{(\sigma_{xx}-\sigma_{yy})^2+(\sigma_{yy}-\sigma_{zz})^2+(\sigma_{zz}-\sigma_{xx})^2+6(\sigma_{xy}{}^2+\sigma_{yz}{}^2+\sigma_{xz}{}^2)\right\}} \tag{6}$$

One direct way to calculate the amplitude of $\sqrt{J_2}$ is:

$$\sqrt{J_{2,a}} \equiv \sqrt{\frac{1}{6}\left\{(\sigma_{xx,a}-\sigma_{yy,a})^2+(\sigma_{yy,a}-\sigma_{zz,a})^2+(\sigma_{zz,a}-\sigma_{xx,a})^2+6(\sigma_{xy,a}{}^2+\sigma_{yz,a}{}^2+\sigma_{xz,a}{}^2)\right\}} \tag{7}$$

Eq.(7) is applicable for proportional loading, where all the stress components vary proportionally. However, when the stress components vary non-proportionally (for example, with phase shift between the stress components), Eq.(7) gives the same result with that of proportional loading condition. In fact, the non-proportionality has influence on the shear stress amplitude generated by multiaxial loading. Therefore, a new methodology is needed.

The longest chord (LC) approach is one of the well-known approaches as summarized by Papadopoulos [9], which defines the shear stress amplitude as half of the longest chord of the loading path, denoted as *D/2*.

The MCC approach [9, 10] defines the shear stress amplitude as the radius of the minimum circle circumscribing to the loading path. On the basis of MCC approach, a new approach, called the minimum circumscribed ellipse (MCE) approach [6], was proposed to compute the effective shear stress amplitude taking into account the non-proportional loading effect. The load traces are represented and analyzed in the transformed deviatoric stress space, where each point represents a value of $\sqrt{J_2}$ and the variations of $\sqrt{J_2}$ are shown during a loading cycle. The schematic representation of the MCE approach and the relation with the minimum circumscribed circle (MCC) approach are illustrated in Fig. 2.

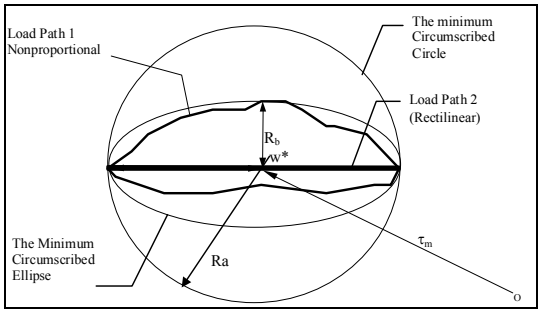


Fig. 2. The MCC and MCE circumscribing to shear stress traces, R_a and R_b are the major and minor radius of MCE, respectively.

The idea of the MCE approach is to construct a minimum circumscribed ellipse that can enclose the whole loading path throughout a loading block in the transformed deviatoric stress space. Rather than defining $\sqrt{J_{2,a}} = R_a$ by the minimum circumscribed circle (MCC) approach, a new definition of $\sqrt{J_{2,a}} = \sqrt{R_a^2 + R_b^2}$ was proposed [6], where R_a and R_b are the lengths of the major semi-axis and the minor semi-axis of the minimum circumscribed ellipse respectively. The ratio of R_b/R_a represents the non-proportionality of the shear stress path. The important advantage of this new MCE approach is that it can take into account the non-proportional loading effects in an easy way.

As shown in Fig. 2, for the non-proportional loading path 1, the shear stress amplitude is defined as $\sqrt{J_{2,a}} = \sqrt{R_a^2 + R_b^2}$. For the proportional loading path 2, it is defined as $\sqrt{J_{2,a}} = R_a$, since R_b is equal to zero (rectilinear loading trace).

6. RESULTS AND DISCUSSIONS

Comparison of local stress-strain responses under different loading paths

The local cyclic elastic-plastic stress/strain responses are evaluated using ABAQUS finite element code. Isoparametric solid element C3D20R with 20 nodes and reduced integration points was used. The FE mesh has 1944 elements and 8809 nodes. Kinematic hardening model with von Mises yield criterion and associative flow rule was used for elastic-plastic FEA.
With the linear kinematic hardening model, the cyclic stress/strain responses get stabilized in the initial 2 loading cycles.
The FEM analyses showed that the cyclic stress-strain responses are different under different loading paths. The stress-strain ranges of the stabilized cycle can be used for life predictions.

Due to space limit, only the local cyclic stress-strain responses results for case1 and case4 are shown and compared in this section. The tensile stress σ22 and tensile strain ε22 at the critical point of the specimen under case 1 loading history is shown in Fig. 3.

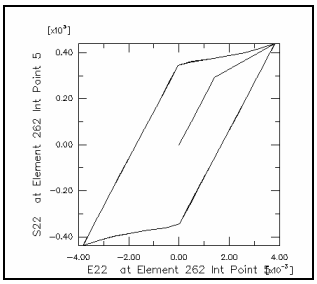


Fig. 3. Hysteretic loop of tensile stress σ_{22} and tensile strain ε_{22} under loading case 1.

The stress path of tensile stress σ_{22} with shear stress τ_{23} under loading case 1 is shown in Fig. 4. It is shown that the local stress path of loading case 1 is not a linear path, because of the cyclic plastic deformation.

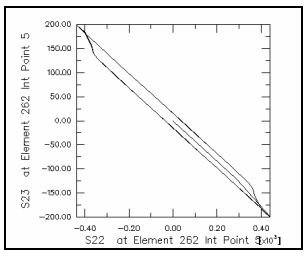


Fig. 4. Stress path of tensile stress σ_{22} with shear stress τ_{23} under loading case 1.

The tensile stress σ22 and tensile strain ε22 at the critical point of the specimen under case 4 loading history is shown in Fig. 5.

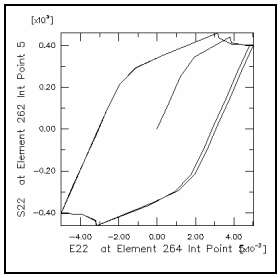


Fig. 5. Hysteretic loop of tensile stress σ_{22} and tensile strain ε_{22} under loading case 4.

The stress path of tensile stress σ_{22} with shear stress τ_{23} under loading case 4 is shown in Fig. 6.

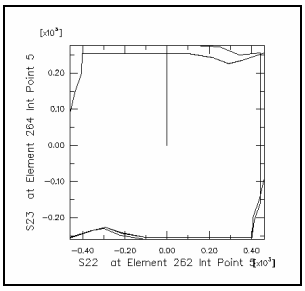


Fig. 6. Stress path of tensile stress σ_{22} with shear stress τ_{23} under loading case 4.

Compared with the loading paths in the table 3, it is shown that the local stress paths have some derivation from the loading paths, due to the interaction of the local normal and shear stresses with plastic deformations.

Comparison of predicted and experimental lives

The lives of the specimens of 42CrMo4 steel subjected to various loading paths were predicted with the improved ASME code approach of Eqs.(4-5). For 42CrMo4 steel, the material constant of additional hardening α is 0.188 as correlated from experimental results by Chen et al [11]. The non-proportionality factor F_{NP} is calculated for each loading path by the MCE approach as described in detail in Ref.[6]. For each loading path shown in the table 2, a minimum circumscribed ellipse is found to enclose the strain path, then the non-proportionality factor F_{NP} is calculated as $F_{NP} = R_b / R_a$, where R_b and R_a are the minor and major radius of the ellipse, respectively.

Fig. 7 and 8 show the comparisons of the experimental fatigue life against the predicted results without and with modification for non-proportional effects, respectively.

It is shown that the predictions with modified equivalent strain range of the ASME code (Fig. 8) have good accuracy by comparison with experimental results, where the dashed lines represent the error band of factor 2.

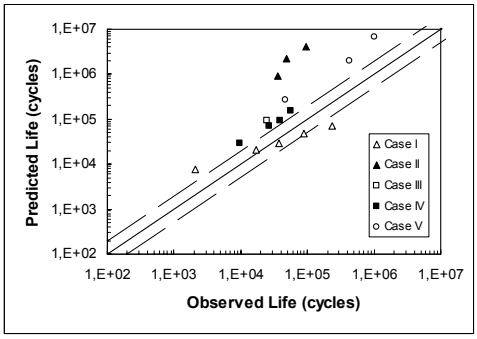


Fig. 7. Comparison of experimental fatigue life with predicted results by the equivalent strain range of the ASME code.

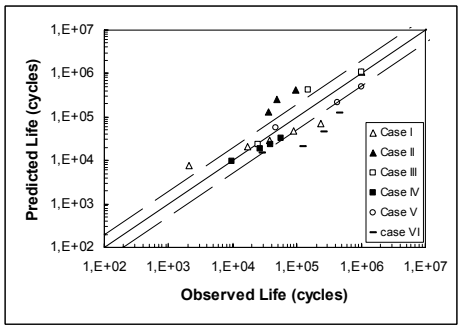


Fig. 8. Comparison of experimental fatigue life with predicted results by modified equivalent strain range of the ASME code.

The stress invariant based approach Eq.(6) is also applied for the life predictions, Fig. 9 shows the comparisons of the experimental fatigue life against the predicted results.

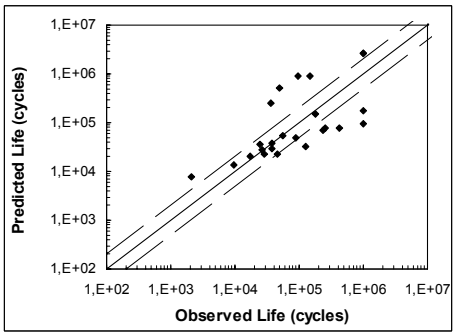


Fig. 9. Comparison of experimental fatigue life with predicted results by stress invariant-based approach with the MCE method for evaluating the shear stress amplitude.

7. CONCLUSIONS

The local cyclic stress/strain states are influenced by the multiaxial loading paths, due to the interactions between the normal stress and shear stress during cyclic plastic deformation. Simulations by finite element method are helpful to understand the evolutions of local cyclic stress/strain, and good fatigue life prediction can be made by using the stabilized local cyclic stress/strain parameters.

The simple and easy of use approaches, such as the equivalent strain range of ASME code and the stress invariant - based approach, can provide good predictions of fatigue life by some modifications for non-proportional effects.

ACKNOWLEDGEMENTS

Financial support from the Fundação para Ciência e Tecnologia (FCT) is acknowledged.

REFERENCES

[1] Socie, D.F. and Marquis, G.B., "Multiaxial Fatigue", Society of Automotive Engineers, Warrendale, PA, (2000).
[2] Ponter, A.R.S. and Carter, K.F., "Shakedown state simulation techniques based on linear elastic solutions", Comput. Methods Appl. Mech. Engrg., 140, 259-279 (1997).
[3] Ellyin,F., "Fatigue Damage, Crack Growth and Life Prediction", Chapman & Hall, (1997).
[4] ASME Code Case N-47-23 (1988) Case of ASME Boiler and Pressure Vessel Code, American Society of Mechanical Engineers.
[5] Itoh, T. and Miyazaki, T. (2001) "A damage model for estimating low cycle fatigue lives under non-proportional multiaxial loading", Proceedings of the 6th International Conference on Biaxial/Multiaxial Fatigue & Fracture, Edited by M. de Freitas, Lisbon, June 25-28, pp. 503-510.
[6] M.de Freitas, B. Li and J.L.T. Santos (2000) Multiaxial Fatigue and Deformation: Testing and Prediction, ASTM STP 1387, S. Kaluri and P.J. Bonacuse, Eds., American Society for Testing and Materials, West Conshohocken, PA, pp.139-156.
[7] G. Sines (1959) Metal Fatigue, (edited by G. Sines and J.L.Waisman), McGraw Hill, New York, pp.145-169.
[8] B. Crossland (1956) Proc. Int. Conf. on Fatigue of Metals, Institution of Mechanical Engineers, London, pp.138-149.
[9] I.V. Papadopoulos (1998) Fatigue & Fracture of Engineering Materials & Structures, Vol. 21, pp. 269-285.
[10] Dang-Van, K. (1993) Advances in Multiaxial Fatigue, ASTM STP 1191, D.L. McDowell and R. Ellis, Eds., American Society for Testing and Materials, Philadelphia, pp.120-130.
[11] Chen, X., Gao Q. and Sun, X.F. (1996) "Low-Cycle Fatigue Under Non-proportional Loading", Fatigue Fract. Engng Mater Struct, 19, No. 7, pp.839-854.